ARTICLE

Electronic Structure of Thiolate-Covered Gold Nanoparticles: $Au_{102}(MBA)_{44}$

Yan Li,[†,*] Giulia Galli,[†] and François Gygi[‡]

[†]Department of Chemistry and [‡]Department of Applied Science, University of California, Davis, California 95616

ABSTRACT We present first principles, density functional theory (DFT) calculations of the structural and electronic properties of thiolate-protected gold nanoparticles [$Au_{102}(MBA)_{44}$] that have been recently crystallized and measured by X-ray diffraction. Our calculations yield structural properties in very good agreement with experiment and reveal the impact of thiolate adsorption on both the surface geometry and the electronic structure of the gold core; in particular, within DFT we observe the emergence of an energy gap of about 0.5 eV, upon MBA adsorption. Using a localized orbital analysis, we characterize the electron distribution in the nanoparticle and provide insight into the bonding of thiolates on curved gold surfaces.

KEYWORDS: DFT · electronic structure · gold cluster · thiolates · charge transfer

Thiolate (RS-) group covered gold nanoparticles have been a topic of intense interest recently, not only because of their potential as chemical or biological sensors, and as organic electronic components, but also because of novel and peculiar properties of their organic/metal interfaces, compared to those involving a flat metal substrate. For example, gold core nanoparticles such as $Au_{25}(RS)_{18}$ and $Au_{38}(RS)_{24}$ have been extensively studied both experimentally[1,2] and theoretically,[2−6] and in general good agreement has been found between measured and computed structural and optical properties.

Recently, Jadzinsky *et al.*[7] reported the successful crystallization and X-ray measurements of a *p*-mercaptobenzoic acid (*p*-MBA)-protected gold nanoparticle containing 102 gold atoms and 44 *p*-MBAs. This measurement revealed that the thiolate groups form linear RS−Au−SR motifs (called "staple" motifs) on the nanoparticle surface, in contrast to the accepted, standard model for flat surfaces, in which thiolates form single covalent bonds with the close-packed underlying substrate. The work of ref 7 is the first complete determination of the structure of a thiolate-covered gold nanoparticle, and it represents one of the few cases where the atomic structure of a nanoparticle is completely and unambiguously determined. It thus offers a unique opportunity to carry out theoretical investigations at the nanoscale where a clear, one to one correspondence between theory and experiment can be established.

In this paper, we analyze the electronic structure of the newly crystallized gold nanoparticles and we elucidate the bonding properties of their organic/inorganic interface, by means of a series of first principles, density functional theory (DFT) calculations. Our results show that the crystal of thiolate-covered gold cluster is a semiconductor, with enhanced stability of interface Au−S bonds, with respect to the case of flat surfaces. Adsorbate molecules exert "pull-out" forces on the surface atoms and the bonding character of the interface indicates donation of electrons from gold to the adsorbates and the presence of an electronically highly stable gold core.

RESULTS AND DISCUSSION

Structural Properties. Figure 1 shows the distribution of atomic distances from the center of the cluster for Au and S atoms, as well as the distribution of Au−Au distances. The X-ray data[7] and our DFT geometry optimization results[8] show excellent overall agreement, confirming the stability of the experimentally determined structure. The gold atoms can be grouped into three shells:[7] 39 gold atoms, within 5.5 Å from the cluster center, constitute the inner core (or first shell) which does not interact with sulfur atoms; 40 gold atoms in the next shell (second shell), within a radius of 5.5−6.5 Å,

*Address correspondence to ynli@ucdavis.edu.

Received for review June 3, 2008 and accepted August 05, 2008.

Published online August 21, 2008. 10.1021/nn800340f CCC: $40.75

TABLE 1. Calculated Bond Lengths and Bond Angles of $Au_{102}(MBA)_{44}$. Au^2 and Au^3 Indicate Gold Atoms in the Second and Third Shells of the Cluster (See also Figure 1)

bond length (Å)		bond angle (deg)			
Au^2-S	Au^3-S	$S-Au^3-S$	Au^2-S-Au^3	$C-S-Au^2$	$C-S-Au^3$
2.34−2.57	2.26−2.34	162.2−174.3	80.0−104.7	108.3−123.0	103.0−115.8

are connected to the RS−Au−SR "staple" motifs through a Au−S bond; the remaining 23 gold atoms in the outermost, third shell, within a radius of 7.5−8.0 Å, interact with two sulfur atoms and form so-called "staple" motifs (see also Figure 1). The computed Au−S bond lengths and sulfur-related bond angles are listed in Table 1. The average length of Au−S bonds participating in the staple motif (2.31 Å) is shorter than that of Au−S bonds involving a gold atom from the second shell (2.42 Å). The average C−S−Au angle is 110.7°, indicating a sp^3-like hybridization of sulfur atoms in the "staple" motif, although pπ−pπ interactions and pπ−dπ-type bonding are also expected among S, C, and Au atoms.

One of the purposes of our work is to understand the impact of adsorbate molecules on the geometry and electronic structure of the underlying gold cluster. Figure 2 shows the DFT-optimized geometry of an isolated Au_{102} nanoparticle viewed along the central 5-fold axis, with gold atoms in successive shells labeled in different colors. The structure of the isolated Au_{102} cluster was optimized starting from the coordinates determined experimentally for the $Au_{102}(MBA)_{44}$ crystal. Upon adsorption of the 44 MBA radicals, the outermost gold shell is lifted outward to form "staple" motifs, with a maximum displacement $|\Delta r|_{max} = 1.75$ Å where $\Delta r \equiv r_{fin} - r_{ini}$. This is consistent with the results of *ab initio* molecular dynamics simulation of methylthiolate (MT) on Au(111),[9] showing that a single gold atom is pulled out of the surface by about 2.0 Å and shared by two MTs. However, a smaller average displacement was found in our case ($|\Delta r|_{avg} = 0.83$ Å), because the curvature of the nanoparticle facilitates the approach of surface gold atoms to the adsorbed molecules. The displacement of Au atoms induced by the presence of adsorbates decreases inside the cluster, and $|\Delta r|_{avg}$ is 0.27 Å and 0.19 Å for gold atoms in the second and innermost shell, respectively.

Electronic Properties. Adsorption of MBA radicals onto the gold cluster not only substantially changes the surface geometry of the nanoparticle, but also modifies its electronic structure, especially the single particle energies near the Fermi level (E_F). Figure 3 shows the electronic density of states (DOS) of the $Au_{102}(MBA)_{44}$ nanoparticle. For energies $E - E_F < -7$ eV, the main contribution to the DOS comes from the molecular orbitals of the MBAs, although the sharp peaks found in the DOS of the free molecule are now broadened because of the different configurations adopted by the adsorbed MBAs, and the interactions among neighboring MBAs and with the gold cluster. In the vicinity of the Fermi level, the DOS shows contributions from both the MBAs and the underlying gold cluster, indicating significant hybridization between Au and S orbitals. Most interestingly, a finite energy gap (~0.48 eV) appears between the valence band and the conduction band of the crystal, while in the isolated Au_{102} cluster the gap between the highest occupied molecular orbital (HOMO) and the lowest unoccupied molecular orbital (LUMO) is smaller than 0.16 eV, as shown in the inset of Figure 3. The square moduli of HOMO and LUMO wave functions of $Au_{102}(MBA)_{44}$ (not shown) indicate that the electron distribution associated with these states is mainly localized on the gold core and interface sulfur atoms. Although the calculation of optical spectra is beyond the scope of the present work (due to the large size of the system considered here), we note that symmetry arguments and the finite overlap found between the square moduli of the HOMO and LUMO indicate that the gap found here may be optically active.

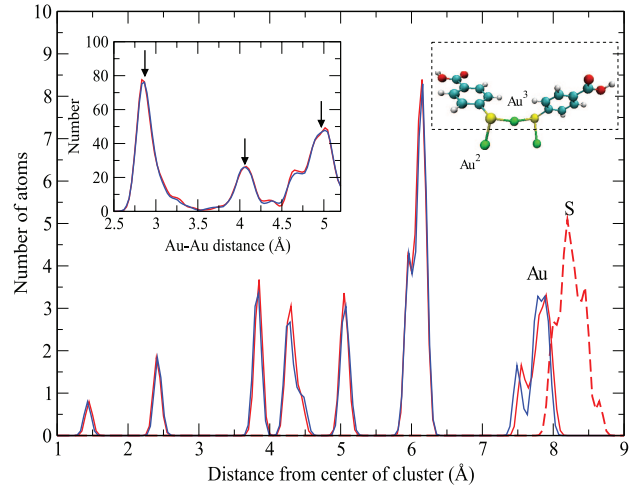

Figure 1. Distribution of distances from the center of the $Au_{102}(MBA)_{44}$ cluster. (Inset) Distribution of Au−Au distances with arrows indicating the experimental Au−Au distances of the first, second, and third nearest neighbors. X-ray data are shown in red for Au (solid curves) and S (dashed curve) while scaled DFT optimized distances for Au are in blue.[8] See Table 1 for calculated Au−S distances. Also shown is a "staple" motif (enclosed in dashed rectangle) with two connecting gold atoms in the second shell.

The emergence of a sizable HOMO−LUMO energy gap has been observed in similar organic-covered gold nanoparticles, both experimentally and theoretically. Chen et al.[10] studied monodisperse gold nanoparticles covered by short-chain alkanethiolates, with diameter ranging from 1.1 to 1.9 nm, and inferred a HOMO−LUMO gap of 0.4−0.9 eV from near-infrared spectroscopic data. An energy gap of about 0.9−1.5 eV was calculated for the $Au_{25}(SR)_{18}$ clusters and $Au_{38}(SR)_{24}$ clusters from DFT studies,[2,4−6] and was found to be closely related to the value of the optical band edge. A recent DFT study on a MT-covered Au_{38}

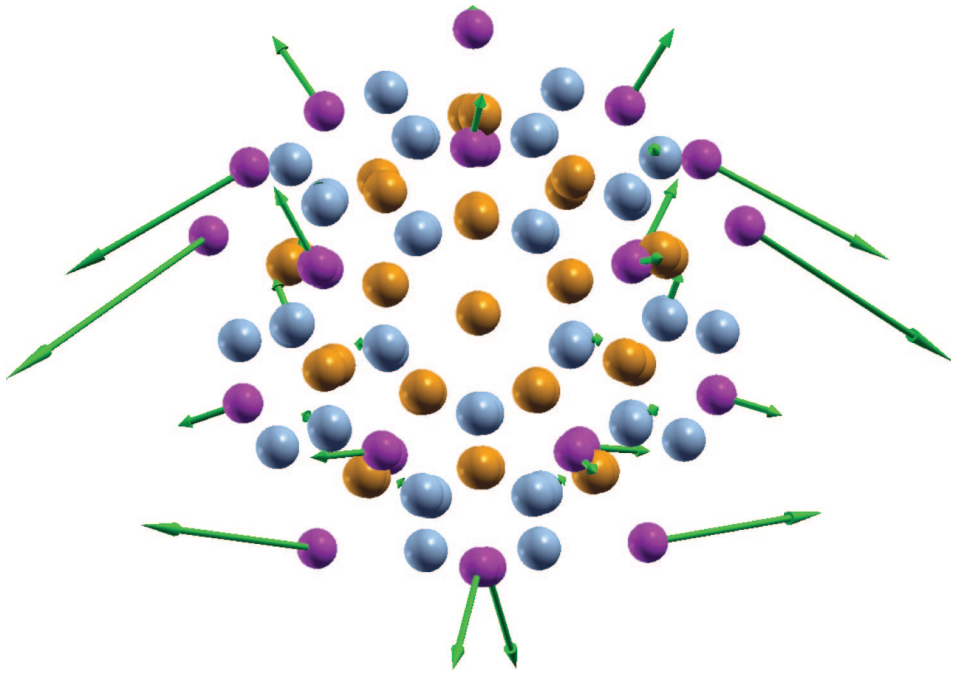

Figure 2. DFT-optimized geometry for the isolated Au_{102} cluster viewed along the central axis. Arrows indicate magnitude and direction of the displacements of Au atoms upon adsorption of 44 MBA radicals. Spheres represent Au atoms in successive shells interacting with zero (orange), one (cyan), or two (magenta) MBA radicals, respectively.

cluster[6] also shows the opening of a significant HOMO−LUMO gap upon formation of a single "staple" motif on the cluster surface; such a gap widens as more "staples" are added. The increase of the energy gap with coverage is consistent with our findings. We optimized the structure of the $Au_{102}(MBA)_2$ cluster, in which a single MBA "staple" motif was considered, and we found a HOMO−LUMO gap of 0.22 eV, much smaller than the value of 0.48 eV, computed in the $Au_{102}(MBA)_{44}$ crystal.

To investigate the influence of the type of adsorbate molecules on the gold nanoparticle electronic properties, we computed the electronic structure of $Au_{102}(MT)_2$ and found a gap (0.19 eV) almost identical to that of $Au_{102}(MBA)_2$; this suggests that the energy gap is not sensitive to the type of thiolates employed. Indeed, a close inspection of the HOMO and LUMO wave functions of both systems show that the HOMOs mainly originate from hybrids obtained from pπ wave functions of the sulfur atoms and dπ wave functions of the connecting gold atoms; the LUMOs instead solely originate from gold atom wave functions (see also Figure 4). Therefore, even though aryl thiolates have a much smaller energy gap than alkyl thiolates in the gas phase, thiolate-covered gold nanoparticles exhibit energy gaps of very similar magnitudes, irrespective of the type of adsorbates. However, the presence of an aromatic ring in aryl thiolates changes the spatial charge distribution of electrons, with respect to alkyl thiolates, and this is expected to change induced surface dipoles and the position of energy levels relative to vacuum, and thus ionization potential and electron affinity. We note that similar conclusions to those drawn here on the insensitivity of energy gaps to adsorbate types were obtained in voltammetry measurements, of electrochemical energy gaps for Au_{38} clusters covered either by hexanethiolates (C_6) or phenylethanethiolates (PhC_2).[11]

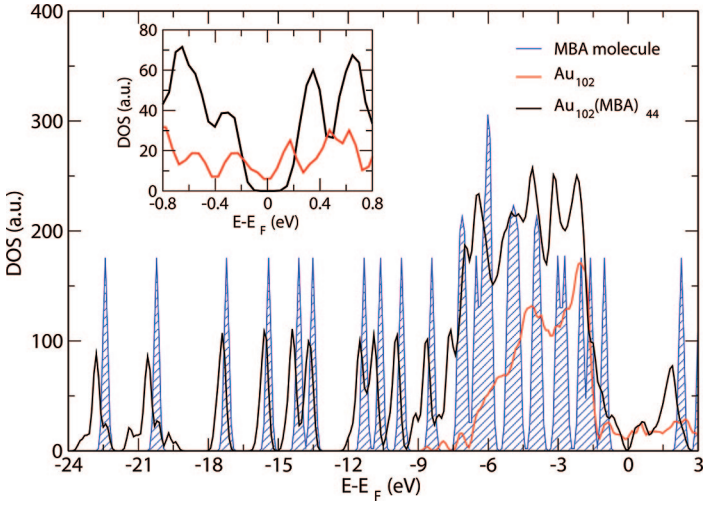

Figure 3. Electronic density of states (DOS) of the gas-phase MBA molecule, the isolated Au_{102} cluster and the $Au_{102}(MBA)_{44}$ nanoparticle (with a Gaussian broadening of 0.1 eV). The energy levels of the gas-phase molecule and the isolated Au_{102} cluster have been aligned by taking the vacuum level as the reference energy; the energy levels of the isolated Au_{102} cluster and the $Au_{102}(MBA)_{44}$ nanoparticle have been aligned by assuming the same HOMO−LUMO midgap. Inset shows a close-up view near the Fermi level (with a Gaussian broadening of 0.05 eV), indicating a finite energy gap of about 0.5 eV for $Au_{102}(MBA)_{44}$.

To characterize the bonding nature of thiolates to gold surface atoms, we computed maximally localized Wannier functions (MLWFs)[12,13] for the occupied bands of the $Au_{102}(MBA)_{44}$ crystal. MLWFs are analogous to the Boys orbitals[14] commonly used in quantum chemistry to describe chemical bonds. Wannier Functions are obtained from the eigenstates of the Hamiltonian by a unitary transformation; their spreads in real space are then minimized to obtain maximally localized orbitals. The procedure of ref 13 was adopted for the spread minimization. The distribution of MLWF centers within a radius of 9 Å from the center of the cluster is illustrated in Figure 5. The MLWFs can be divided into two subgroups, one containing orbitals with small spreads

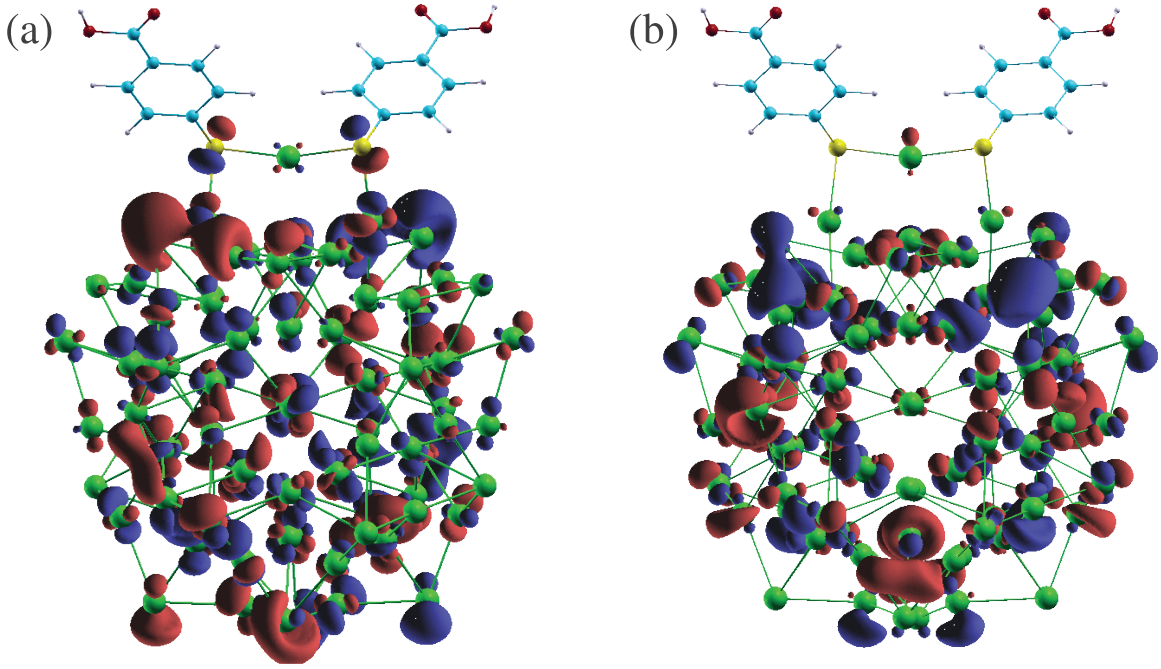

Figure 4. Isosurfaces of square moduli for (a) HOMO and (b) LUMO wave functions of $Au_{102}(MBA)_2$.

(<1.5 Å; 510 MLWFs in total) and one composed of orbitals with large spreads (>2 Å; 29 MLWFs in total). As shown in the upper panel of Figure 5, the functions of the first subgroup have centers overlapping with the coordinates of the gold atoms. A careful inspection of these 510 MLWFs reveals that they exactly correspond to localized d-orbitals centered on the 102 gold atoms. On the other hand, the MLWFs belonging to the second subgroup are centered between gold atoms and have an s-orbital nature, as indicated by their phase. The centers of the large-spread MLWF centers have radii within three, distinct, narrow ranges: $r = 0.83$, $r = 1.58$, and 4.10 Å $< r <$ 4.67 Å (see lower panel of Figure 5). In contrast, a similar analysis for the isolated Au_{102} cluster shows that 51 MLWFs exhibit large spreads and have a broader radial distribution within the whole nanoparticle, all the way to the surface of the cluster. The reason why 29 MLWFs have large spreads in the thiolate-covered cluster, instead of 51, as in the bare gold nanoparticle, is related to the bonding character of the 44 MBA radicals to the gold surface, each of which lacks one electron to fill its eight-electron outer shell. We note that the 44 total MBA radicals not only form single RS−Au−SR "staple" motifs, but are also engaged in double "staple" motifs (RS−Au−S−Au−RS). In fact, there are 19 single "staple" motifs and 2 double "staple" motifs, which add up to $19 \times 2 + 2 \times 3 = 44$ MBA radicals and $19 \times 1 + 2 \times 2 = 23$ Au atoms in the outmost shell.

It was suggested[7] that 44 of Au s-electrons are donated to the thiolates while the remaining Au s-electrons form a filled-shell of 58 electrons. This is expected to contribute to the stability of the thiolate-covered nanoparticle as it is known that 58 electrons form a stable electronic shell structure.[15,16] This interpretation is supported by our MLWF analysis. We also simulated the electron distribution of an effective one-electron potential $U(r) = -U_0/(1 + \exp[(r - r_0)/\sigma])$ with a broadening width $\sigma = 0.2$ au. U_0 is the Au work function (5.21 eV) and $r_0 = r_s N^{1/3} = 11.65$ au is the effective radius of a gold cluster containing N delocalized electrons, with $r_s = 3.01$ au and $N = 58$. The MLWF center distribution of such a simplified model turned out to be strikingly similar to that found in $Au_{102}(MBA)_{44}$, supporting the hypothesis that 44 Au s-electrons are donated to the MBA adsorbates.

Energetic Stability. To further analyze the stability of thiolate-covered gold nanoparticles, we computed the adsorption energy of MBA radicals to a Au_{102} cluster; the adsorption energy per MBA radical, E_{ad}, is defined from the difference in the total energy of the $Au_{102}(MBA)_{44}$ crystal (including both enantiomers and the 24 water molecules, some of which are hydrogen-bonded to the -COOH termini of MBAs) and the sum of the total energies of isolated components:

$$-88E_{ad} = E_{tot}[Au_{102}(MBA)_{44}\ \text{crystal}] - \{2E_{tot}[Au_{102}] + 88E_{tot}[MBA] + 24E_{tot}[H_2O]\} \quad (1)$$

where $E_{tot}[Au_{102}(MBA)_{44}\ \text{crystal}]$, $E_{tot}[Au_{102}]$, $E_{tot}[MBA]$, and $E_{tot}[H_2O]$ are the total energies of the $Au_{102}(MBA)_{44}$ crystal, of an optimized isolated Au_{102} cluster, of an isolated MBA radical and of an isolated water molecule, respectively. This yields an adsorption energy of 1.96 eV/MBA. In comparison, for a single MBA "staple" motif on the cluster, the adsorption energy was calculated to be

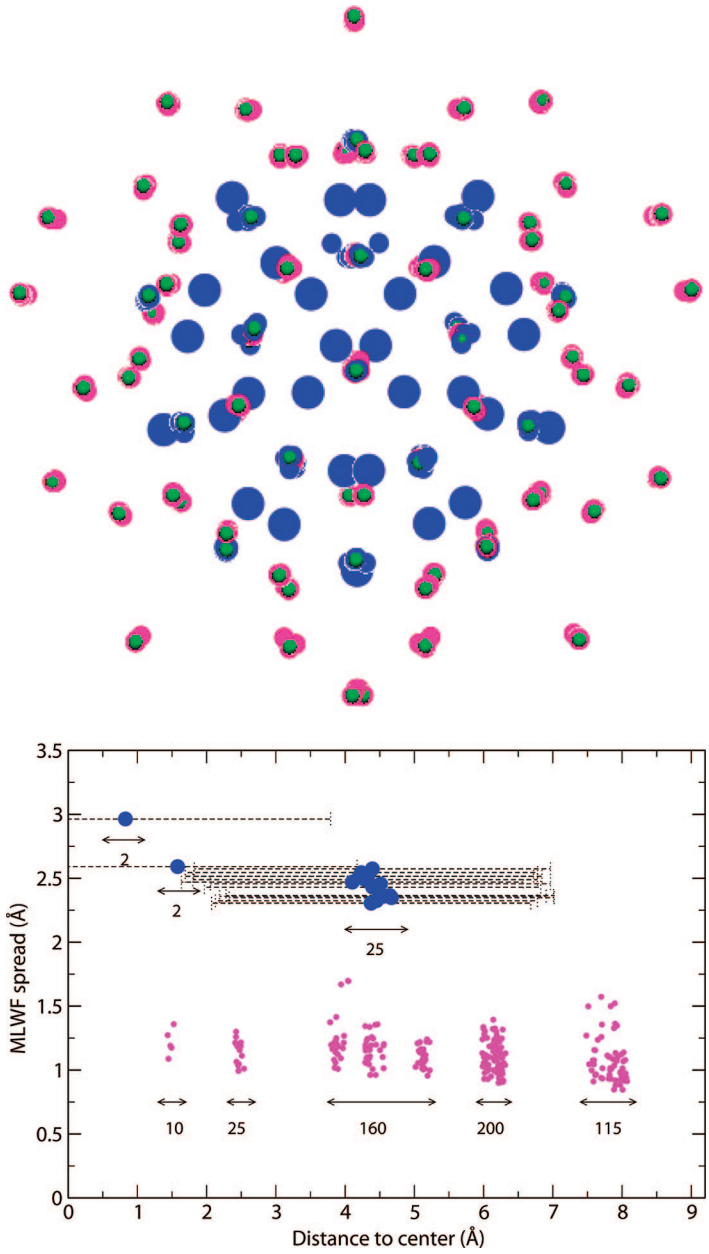

Figure 5. Distribution of MLWF centers of $Au_{102}(MBA)_{44}$ (see text). (Upper panel) MLWF centers with large spreads (>2 Å; blue points) and small spreads (<1.5 Å; magenta points) shown in real space. Au atoms are represented by green spheres and other atoms are omitted for clarity. (Lower panel) Spreads of MLWF centers as a function of the radial distance. Values under the arrows indicate the number of MLWF centers of the corresponding subgroups. Large spreads are indicated by horizontal bars.

slightly higher (~2.16 eV/MBA). The decrease of E_{ad} at high coverage can be explained by the steric repulsion between MBA radicals as the number of adsorbate molecules increases, and by the limited freedom for the underlying gold core atoms to relax. This tendency is consistent with that observed in a DFT study of MT-covered Au_{38} cluster,[6] although a much larger adsorption energy was found for $Au_{38}(MT)_2$ (~3.44 eV/MT). This may be due to the O_h symmetry assumed for the isolated Au_{38} cluster in those calculations, which yields a higher total energy than that of the disordered, minimum energy configuration.

Finally, we studied MBA radicals bound to a defect-free Au(111) surface or to an adatom on the flat surface, forming a "staple" motif. For the defect-free Au(111) surface, a $(3 \times 3)R30°$ unit cell with a four-layer slab was used, containing nine gold atoms per layer, and a uniform k grid of $3 \times 3 \times 1$ was adopted. An adsorption energy of 1.26 eV was found for adsorption at the fcc site, slightly shifted to the bridge site, with an average Au−S bond length of 2.47 Å. In contrast, at full coverage, the most stable adsorption configuration for the MBA radical was found at a bridge site slightly shifted to the fcc site, and the averaged Au−S bond length was calculated to be about 2.49 Å, consistent with previous DFT calculations of diphenyl-thiolate on Au(111) surfaces.[17] For the "staple" motif, a $p(7 \times 2)$ unit cell, containing 28 gold atoms per layer, was used to ensure minimum interaction between the MBA pairs and two special k points were used for the Brillouin zone sampling. The adsorption energy per MBA, including the formation energy of an Au adatom on the clean Au(111) surface, is defined as

$$-2E_{ad} = E_{tot}[\text{MBA}-\text{Au}-\text{MBA}/\text{Au}(111)] - \{E_{tot}[\text{Au}(111)] + 2E_{tot}[\text{MBA}] + E_{tot}[\text{Au bulk}]\} \quad (2)$$

and was calculated to be 1.59 eV/MBA. The terms on the right-hand side of eq 2 are the total energies of a staple motif formed on the Au(111) surface, of a defect-free Au(111) surface, of isolated MBA radicals, and of a bulk Au atom, respectivly. The average bond length d_{Au-S} was calculated to be 2.34 Å for Au−S bonds in the "staple" motif and 2.55 Å for the shortest Au−S bonds to the close-packed substrate. The increase of adsorption energy in the presence of an adatom is consistent with previous DFT calculations[6,9,18,19] and experimental measurements,[9,20,21] on benzenethiols and alkanethiols on Au(111) surfaces, and highlights the importance of surface defects at organic/metal interfaces. We note that the Au−S bond lengths of the "staple" motif in $Au_{102}(MBA)_2$ (d_{Au-S} = 2.35 Å) are similar to those found on Au(111), while the Au−S bonds to gold atoms in the second shell (d_{Au-S} = 2.41 Å) are shorter than those to the Au(111) substrate, consistent with the larger adsorption energy in the case of the cluster. This indicates that a finite curvature enhances the energetic stability of the Au−S binding.

CONCLUSIONS

In summary, we have presented *ab initio* calculations of the structural, electronic, and bonding properties of thiolate-covered gold nanoparticles that have been crystallized in recent experiments. The results of our structural optimization confirm the stability of the experimentally determined structure, and show a ten-

dency of the adsorbate to exert "pull-out" forces on the surface gold atoms. We find that the crystallized structure is a semiconductor with a sizable energy gap (~0.5 eV, within DFT), and electronic states at the valence band maximum and conduction band minimum are extended over the gold nanoparticle core and the interface. This energy gap appears to be insensitive to the type of adsorbate. Our analysis of chemical bonding supports the hypothesis that gold s electrons are donated to the MBA radicals so as to form a highly stable 58-electron, filled electronic shell structure. Finally, comparisons between adsorption energies in the case of gold nanoparticles and flat surfaces show that a finite curvature of the interface enhances the stability of Au−S bonds. After submission of our paper another study of the electronic properties of $Au_{102}(MBA)_{44}$ appeared,[26] whose findings are fully consistent with ours.

COMPUTATIONAL DETAILS

In our calculations, we adopted the Perdew−Burke−Ernzerhof[22] (PBE) approximation to the exchange-correlation energy; we used plane wave basis sets, with a kinetic energy cutoff of 75 Ry, and nonlocal, norm-conserving pseudopotentials to describe the interaction between ionic cores and valence electrons. We used fractional occupation numbers for electrons and a Fermi distribution with $T = 300$ K. We considered unit cells containing two $Au_{102}(MBA)_{44}$ enantiomers, connected by hydrogen bonds through the -COOH terminal groups of MBA radicals and surrounded by 24 water molecules, corresponding to the experimentally observed unit cell.[7] This amounts to 1596 atoms and 6924 valence electrons included in our optimization procedures. The coordinates of either enantiomer can be derived from those of the other by applying an inversion operator and therefore in most of the text we just refer to the properties of one of the enantiomers.

Unit cell parameters and the initial crystal geometry for our structural optimization procedure were taken from the published X-ray data.[7] For computations of the periodic crystal with space group *C*2/*c*, and MLWF analyses, we used the Qbox code.[23] Only the Γ point was included in the sampling of the crystal Brillouin zone. We also carried out calculations using the PWSCF package[24] for an isolated Au_{102} cluster, placed in a fcc cell of lattice parameter $a = 15.87$ Å, and for thiolates adsorbed on the Au(111) surface, using a four-layer slab separated by nine layers of vacuum. The total energies of isolated molecules and radicals were evaluated in a simple cubic cell of $a = 15.87$ Å, and spin-polarized calculations were used for thiolates. Generation of pseudopotentials and other simulation details are the same as in ref 25. Our structural minimization was stopped when all ionic forces acting on Au and S atoms were less than 0.03 eV/Å.

Acknowledgment. This work was funded by NSF Grant No. DMR-0213618 and by DOE/BES Grant No. DE-FG02-06ER46262. F. G. acknowledges support from NSF through grant 0749217. Most of the processing time to support this research was provided on IBM's Blue Gene Watson system through IBM's participation in the DOE INCITE program and we thank Dr. Fred Mintzer for his help and support. Some calculations were performed at the SDSC and NERSC facilities.

Supporting Information Available: Cartesian coordinates for DFT-optimized geometries of the clusters and surface structures in our electronic structure calculations. This material is available free of charge *via* the Internet at http://pubs.acs.org.

REFERENCES AND NOTES

1. Heaven, M.; Dass, A.; White, P.; Holt, K.; Murray, R. Crystal Structure of the Gold Nanoparticle $[N(C_8H_{17})_4][Au_{25}(SCH_2CH_2Ph)_{18}]$. *J. Am. Chem. Soc.* **2008**, *130*, 3754–3755.
2. Zhu, M.; Aikens, C. M.; Hollander, F. J.; Schatz, G. C.; Jin, R. Correlating the Crystal Structure of a Thiol-Protected Au_{25} Cluster and Optical Properties. *J. Am. Chem. Soc.* **2008**, *130*, 5883–5885.
3. Hakkinen, H.; Walter, M.; Gronbeck, H. Divide and Protect: Capping Gold Nanoclusters with Molecular Gold-Thiolate Rings. *J. Phys. Chem. B* **2006**, *110*, 9927–9931.
4. Akola, J.; Walter, M.; Whetten, R.; Hakkinen, H.; Gronbeck, H. On the Structure of Thiolate-Protected Au_{25}. *J. Am. Chem. Soc.* **2008**, *130*, 3756–3757.
5. Pei, Y.; Gao, Y.; Zeng, X. C. Structural Prediction of Thiolate-Protected Au_{38}: A Face-Fused Bi-icosahedral Au Core. *J. Am. Chem. Soc.* **2008**, *130*, 7830–7832.
6. Jiang, D.-e.; Tiago, M.; Luo, W.; Dai, S. The "Staple" Motif: A Key to Stability of Thiolate-Protected Gold Nanoclusters. *J. Am. Chem. Soc.* **2008**, *130*, 2777–2779.
7. Jadzinsky, P. D.; Calero, G.; Ackerson, C. J.; Bushnell, D. A.; Kornberg, R. D. Structure of a Thiol Monolayer-Protected Gold Nanoparticle at 1.1 Å Resolution. *Science* **2007**, *318*, 430–433.
8. The distance in the DFT results was scaled by 1.015 in the plot to compenstate for the artificial expansion of Au-Au distance because of the use of GGA pseudopotential. In contrast, the bulk equilibrium lattice constant from GGA is about 2.5% larger compared to experiments.[25]
9. Mazzarello, R.; Cossaro, A.; Verdini, A.; Rousseau, R.; Casalis, L.; Danisman, M. F.; Floreano, L.; Scandolo, S.; Morgante, A.; Scoles, G. Structure of a CH_3S Monolayer on Au(111) Solved by the Interplay between Molecular Dynamics Calculations and Diffraction Measurements. *Phys. Rev. Lett.* **2007**, *98*, 016102.
10. Chen, S.; Ingram, R. S.; Hostetler, M. J.; Pietron, J. J.; Murray, R. W.; Schaaff, T. G.; Khoury, J. T.; Alvarez, M. M.; Whetten, R. L. Gold Nanoelectrodes of Varied Size: Transition to Molecule-Like Charging. *Science* **1998**, *280*, 2098–2101.
11. Jimenez, V.; Georganopoulou, D.; White, R.; Harper, A.; Mills, A.; Lee, D.; Murray, R. Hexanethiolate Monolayer Protected 38 Gold Atom Cluster. *Langmuir* **2004**, *20*, 6864–6870.
12. Souza, I.; Marzari, N.; Vanderbilt, D. Maximally Localized Wannier Functions for Entangled Energy Bands. *Phys. Rev. B* **2001**, *65*, 035109.
13. Gygi, F.; Fattebert, J.-L.; Schwegler, E. Computation of Maximally Localized Wannier Functions using a Simultaneous Diagonalization Algorithm. *Comput. Phys. Commun.* **2003**, *155*, 1–6.
14. Boys, S. F. Construction of Some Molecular Orbitals to Be Approximately Invariant for Changes from One Molecule to Another. *Rev. Mod. Phys.* **1960**, *32*, 296–299.
15. Knight, W. D.; Clemenger, K.; de Heer, W. A.; Saunders, W. A.; Chou, M. Y.; Cohen, M. L. Electronic Shell Structure and Abundances of Sodium Clusters. *Phys. Rev. Lett.* **1984**, *52*, 2141–2143.
16. Martin, T. P.; Bergmann, T.; Goehlich, H.; Lange, T. Shell Structures of Clusters. *J. Phys. Chem.* **1991**, *95*, 6421–6429.
17. Sun, Q.; Selloni, A.; Scoles, G. Electronic Structure of Metal/Molecule//Metal Junctions: A Density Functional Theory Study of the Influence of the Molecular Terminal Group. *J. Phys. Chem. B* **2006**, *110*, 3493–3498.
18. Gronbeck, H.; Hakkinen, H. Polymerization at the Alkylthiolate-Au(111) Interface. *J. Phys. Chem. B* **2007**, *111*, 3325–3327.
19. Wang, Y.; Hush, N.; Reimers, J. Formation of Gold-Methanethiyl Self-Assembled Monolayers. *J. Am. Chem. Soc.* **2007**, *129*, 14532–14533.

20. Maksymovych, P.; Yates, J. T. Au Adatoms in Self-Assembly of Benzenethiol on the Au(111) Surface. *J. Am. Chem. Soc.* **2008**, *130*, 7518–7519.
21. Yu, M.; Bovet, N.; Satterley, C. J.; Bengió, S.; Lovelock, K. R. J.; Milligan, P. K.; Jones, R. G.; Woodruff, D. P.; Dhanak, V. True Nature of an Archetypal Self-Assembly System: Mobile Au-Thiolate Species on Au(111). *Phys. Rev. Lett.* **2006**, *97*, 166102.
22. Perdew, J. P.; Burke, K.; Ernzerhof, M. Generalized Gradient Approximation Made Simple. *Phys. Rev. Lett.* **1996**, *77*, 3865–3868.
23. Qbox bersion 1.43.2. http://eslab.ucdavis.edu/software/qbox.
24. Baroni, S.; Corso, A. D.; de Gironcoli, S.; Giannozzi, P.; Cavazzoni, C.; Ballabio, G.; Scandolo, S.; Chiarotti, G.; Focher, P.; Pasquarello, A. *et al.* PWSCF and PHONON: Plane-Wave Pseudo-Potential Codes, version 3.2. http://www.pwscf.org, 2007.
25. Li, Y.; Lu, D.; Swanson, S.; Scott, J.; Galli, G. Microscopic Characterization of the Interface between Aromatic Isocyanides and Au(111): A First-Principles Investigation. *J. Phys. Chem. C* **2008**, *112*, 6413–6421.
26. Walter, M.; Akola, J.; Lopez-Acevedo, O.; Jadzinsky, P. D.; Calero, G.; Ackerson, C. J.; Whetten, R. L.; Gronbeck, H.; Hakkinen, H. A Unified View of Ligand-Protected Gold Clusters as Superatom Complexes. *Proc. Natl. Acad. Sci. U.S.A.* **2008**, *105*, 9157–9162.